Tetrahedron 69 (2013) 6262–6268

Contents lists available at SciVerse ScienceDirect

Tetrahedron

journal homepage: www.elsevier.com/locate/tet

Conformational analysis of *E*/*Z*-isomeric pairs of rosuvastatin and its lactonized analogues

Jan Fabris [a,b], Damjan Makuc [c,d], Zdenko Časar [b,e], Janez Plavec [c,d,f,*]

[a] *Cadonic Consultancy Services, LL.C., Cesta na postajo 74, SI-1351 Brezovica pri Ljubljani, Slovenia*
[b] *Lek Pharmaceuticals, d.d., Sandoz Development Center Slovenia, API Development, Organic Synthesis Department, Kolodvorska 27, SI-1234 Mengeš, Slovenia*
[c] *Slovenian NMR Centre, National Institute of Chemistry, Hajdrihova 19, SI-1000 Ljubljana, Slovenia*
[d] *EN-FIST Centre of Excellence, Dunajska cesta 156, SI-1000 Ljubljana, Slovenia*
[e] *Faculty of Pharmacy, University of Ljubljana, Aškerčeva cesta 7, SI-1000 Ljubljana, Slovenia*
[f] *Faculty of Chemistry and Chemical Technology, University of Ljubljana, Aškerčeva cesta 5, SI-1000 Ljubljana, Slovenia*

ARTICLE INFO

Article history:
Received 22 February 2013
Received in revised form 24 April 2013
Accepted 9 May 2013
Available online 14 May 2013

Keywords:
Conformational analysis
Isomerism
NMR
Statins
Drugs

ABSTRACT

Most of the super-statins contain a C=C double bond spacer between the heterocyclic and the chiral dihydroxycarboxylic moieties. The known drugs are *E*-geometric isomers, whereas very little is known about their *Z*-isomeric analogues. This study explains the unusual resonance line broadening observed in ^{1}H NMR spectra of *Z*-isomeric rosuvastatin analogues at room temperature, which originates from dynamic exchange between different conformers. Conformational equilibria and intrinsic preferences of *Z*-isomeric rosuvastatin analogues provide valuable insight into conformational variability that is important for studying potential interactions within the binding site of the enzyme.

1. Introduction

Nowadays cardiovascular diseases (CVD) represent one of the most frequent causes of death worldwide.[1] It is well known that overaccumulation of cholesterol in the organism plays a central role in CVD.[2] The inhibition of enzyme 3-hydroxy-3-methylglutaryl-coenzyme A reductase (HMGR), which is the rate-limiting enzyme in the biosynthesis of cholesterol, effectively lowers the concentration of low density lipoproteins in the blood thus reducing the risk of CVD.[3] The most effective HMGR inhibitors are statins and they represent one of the most valuable therapeutic classes of compounds in the pharmaceutical sector. Statins were discovered as fungal metabolites in the 1970s (e.g., mevastatin[4] and lovastatin[5]) and were soon developed through semi-synthetic analogues (pravastatin[6] and simvastatin[7]) towards fully synthetic compounds named super-statins (fluvastatin,[8] atorvastatin,[9] rosuvastatin[10] and pitavastatin[11]).[12]

Most of the marketed super-statins comprise a C=C double bond as a spacer between the heterocyclic and the pharmacophoric chiral dihydroxycarboxylic moiety. Examples of such compounds are fluvastatin, rosuvastatin and pitavastatin. Even though the presence of a double bond enables the formation of two geometric (*E* and *Z*) isomers, it is important to note that all of the commercial super-statins are *E*-geometric isomers. In general, in biologically active compounds *E*-configuration along C=C double bond is not always most active or preferred in terms of pharmacodynamic properties. There are some commercially available drugs and biologically active compounds with *Z*-configuration along the exocyclic C=C double bonds. Examples of such substances are e.g., cis-cefprozil,[13] lafutidine,[14] many combretastatins[15] and prostaglandins[16] together with their synthetic analogues. During the discovery stage of more potent and efficient super-statins a series of analogues has been prepared and tested for the inhibition of HMGR. The large efforts included also some *Z*-isomeric analogues, which showed only weak in vitro activity in some studies[17] and a complete loss of activity in the others.[18] Interestingly, literature data highlighting the rationale for low activity of *Z*-isomeric statins are scarce. Structural mechanism of inhibition was investigated using X-ray crystal structures of HMGR complexed with different *E*-isomeric statins.[19] Furthermore, the kinetic and thermodynamic characterization of binding to HMGR and inhibition of HMGR by different statins have contributed important details on molecular mechanism for inhibition.[20]

* Corresponding author. Tel.: +386 1 476 0353; fax: +386 1 476 0300; e-mail address: janez.plavec@ki.si (J. Plavec).

0040-4020/$ – see front matter © 2013 Elsevier Ltd. All rights reserved.
http://dx.doi.org/10.1016/j.tet.2013.05.020

We have recently elaborated a new synthetic route to rosuvastatin calcium via Wittig coupling reaction[21] between phosphonium salt of an appropriately functionalized heterocyclic moiety and lactonized statin side chain precursor.[22] An interesting side-product was isolated and characterized as the *Z*-isomeric 4-*O*-TBS protected rosuvastatin lactone ***Z*-1**.[21] Surprisingly, ^{1}H NMR spectrum of this novel rosuvastatin analogue showed broad lines, which could indicate the presence of different rotational conformers. Excited by the observation of unexpected conformational properties of ***Z*-1** in solution at room temperature, we were encouraged to synthesize two more rosuvastatin analogues ***Z*-2** and ***Z*-3** (Fig. 1). All three *Z*-isomeric rosuvastatin derivatives showed broad ^{1}H NMR resonances.

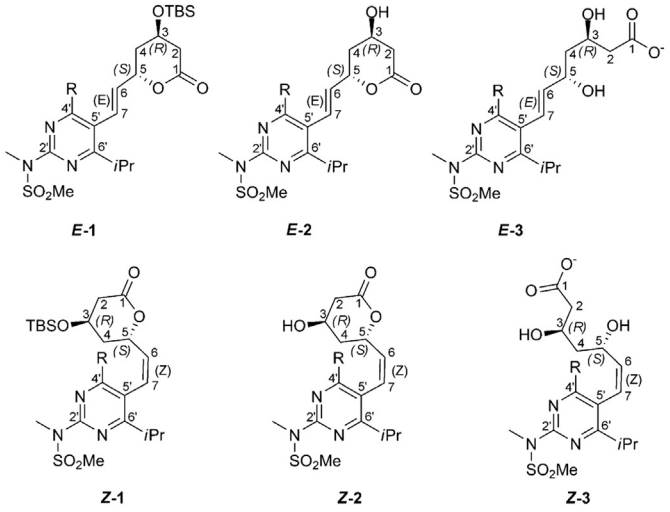

Fig. 1. Chemical structures and atom numbering of 4-*O*-TBS protected rosuvastatin lactone **1**, deprotected rosuvastatin lactone **2** and rosuvastatin calcium **3** (R=*p*-F–C_6H_4).

We hypothesized that at sufficiently low temperature the intramolecular rotations will slow down on the NMR chemical shift time scale and resolved signals will be observed enabling characterization of interconverting rotamers. Temperature-dependent NMR study provided insight into rotational equilibria of *Z*-isomeric analogues in comparison to their *E*-isomers. The chemical structures of rosuvastatin analogues with a linker region between their hydrophobic heterocyclic moieties and chiral dihydroxycarboxylic side chain exhibit several single bonds that could be conformationally flexible. NMR enabled the localization of rotational degrees of freedom and an evaluation of these preferences through van't Hoff analysis. The assessment of the rotational energy barrier from coalescence temperature was complemented by ab initio calculations thus giving a comprehensive insight into conformational features of isomeric pair of rosuvastatin that are important for understanding their physical and biochemical properties.

2. Results and discussion

Compounds ***E*-1**, ***E*-2**, ***E*-3**, and ***Z*-1** were prepared according to the published procedure.[21] In addition, ***Z*-1** was deprotected using tetrabutylammonium fluoride trihydrate and acetic acid to give ***Z*-2**, which was further treated with aqueous NaOH and $CaCl_2$, respectively, to yield *Z*-isomeric rosuvastatin calcium ***Z*-3** (Scheme 1).

Assignments of ^{1}H and ^{13}C NMR resonances for ***Z*-1**, ***Z*-2** and ***Z*-3** were achieved from signal multiplicities, integral values and characteristic chemical shifts from the through-bond correlations in 2D DQF-COSY spectra, through-space correlations in 2D NOESY spectra

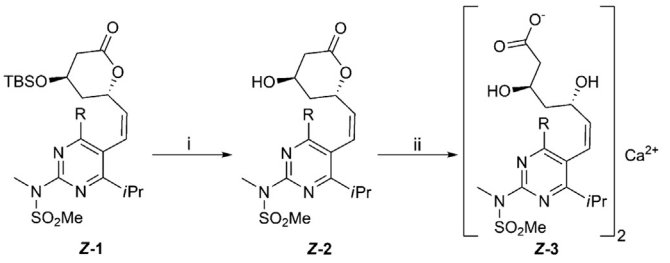

Scheme 1. Reagents and conditions: (i) (^{n}Bu)$_4$NF, AcOH, THF, 0 °C to rt; (ii) NaOH, THF/H_2O, 30 °C then $CaCl_2$ (aq), rt.

as well as from ^{1}H–^{13}C heteronuclear correlations in HSQC and HMBC spectra. The unambiguous ^{1}H and ^{13}C chemical shift assignments of novel compounds ***Z*-2** and ***Z*-3** are reported in the Experimental section.

The comparison of ^{1}H NMR spectra of rosuvastatin ***E*-3** and its isomeric analogue ***Z*-3** showed NMR resonances with similar chemical shifts (Fig. 2). However, remarkable differences in signal line-widths were observed for the two geometric isomers. ***Z*-3** showed broader NMR signals (e.g., $\Delta\nu_{1/2}\approx 8$ Hz for H7) in comparison to its *E*-counterpart ($\Delta\nu_{1/2}\approx 3$ Hz).

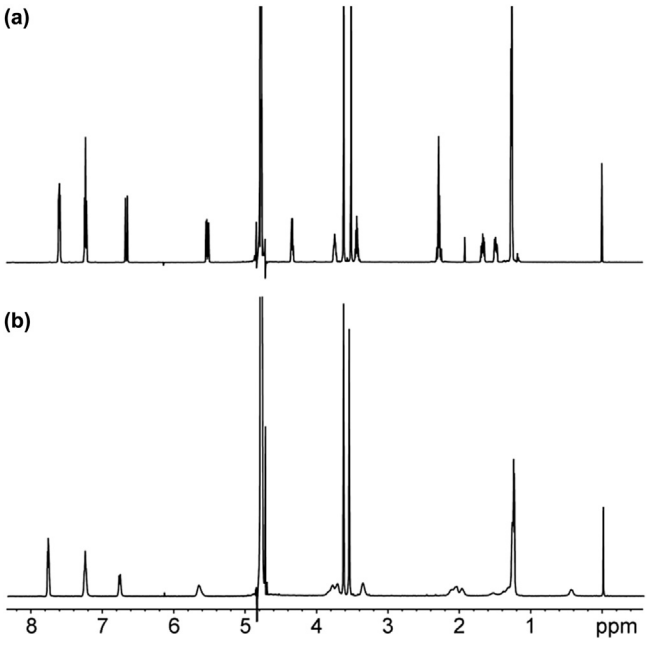

Fig. 2. ^{1}H NMR (600 MHz) spectra of ***E*-3** (a) and ***Z*-3** (b) dissolved in D_2O at 298 K.

Due to the low solubility of rosuvastatin and its derivatives in water and the need to perform NMR experiments at low temperatures different organic solvents were used. Upon cooling of ***Z*-3** in methanol-d_4 to 223 K two sets of sharp and well-resolved signals were observed in the ratio of 5:1, which were labelled as major (M) and minor (m) conformers in solution (Fig. 3). Heating of the sample above the coalescence temperature of ca. 303 K resulted in a single set of signals (Fig. S1). Similarly, two sets of signals were observed for *Z*-isomeric 4-*O*-TBS protected rosuvastatin lactone ***Z*-1** and deprotected *Z*-isomeric rosuvastatin lactone ***Z*-2** in acetone-d_6 at 223 K. The perusal of ^{1}H NMR spectra at 223 K showed interesting differences in multiplicity of H5 and H7 resonances. The $^4J_{H5-H7}$ allylic coupling constant with value of 1.1 Hz was observed for the minor conformer of ***Z*-1** at 223 K in acetone-d_6 (Table 1). In contrast, no $^4J_{H5-H7}$ coupling constant was observed for the major conformer in acetone-d_6. Well-defined differences in allylic

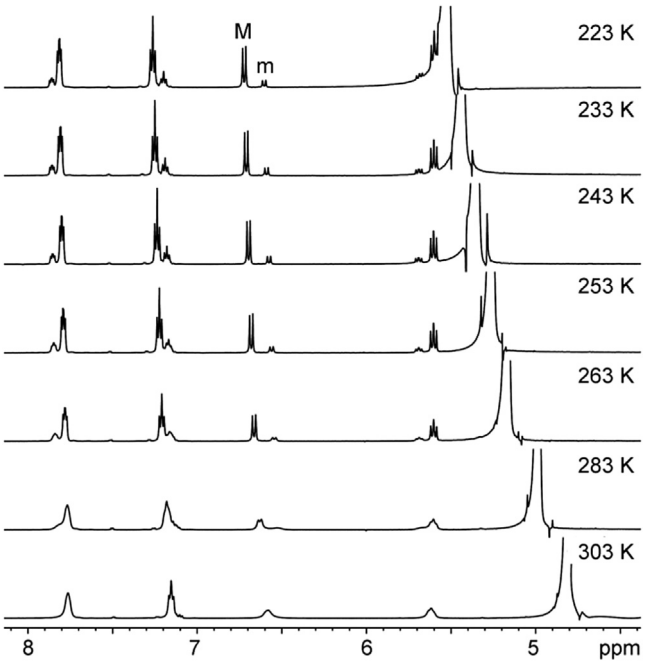

Fig. 3. ^{1}H NMR (600 MHz) spectra of ***Z*-3** dissolved in methanol-d_4 from 223 to 303 K. Labels M and m denote H7 resonances at δ ca. 6.6 ppm corresponding to the major and minor conformers, respectively.

Table 1
^{1}H–^{1}H coupling constants in different solvents at 223 K

Compound	Major conformer (M)			Minor conformer (m)		
	$^3J_{H5-H6}$	$^3J_{H6-H7}$	$^4J_{H5-H7}$	$^3J_{H5-H6}$	$^3J_{H6-H7}$	$^4J_{H5-H7}$
***Z*-1**[a]	10.0	11.2	0.0	9.2	11.3	1.1
***Z*-2**[a]	10.2	11.2	0.0	9.4	11.2	0.8
***Z*-3**[b]	m[c]	11.2	0.0	m[c]	11.7	<0.6[d]
***E*-1**[a]	6.8	16.1	0.9	—	—	—
***E*-2**[a]	7.0	16.1	0.9	—	—	—
***E*-3**[b]	6.8	15.9	<0.6[d]	—	—	—

[a] Compound dissolved in acetone-d_6.
[b] Compound dissolved in methanol-d_4.
[c] Broad multiplet was observed.
[d] J was within the line-width of the resonance.

coupling constants between major and minor conformers suggested the presence of two rotamers along the C5–C6 single bond in ***Z*-1**.

Similar $^4J_{H5-H7}$ coupling constants of 0.8 and 0 Hz were found for the minor and major rotamers of ***Z*-2**, respectively (Table 1). Furthermore, no $^4J_{H5-H7}$ coupling constant was observed for the major rotamer of ***Z*-3** in methanol-d_4 at 223 K. Broad multiplet for H7 signal was observed for the minor rotamer of ***Z*-3** and the corresponding $^4J_{H5-H7}$ allylic coupling constant was within the line-width of the resonance. Rotations along the C5–C6 and C5′–C7 single bonds allow rosuvastatin derivatives ***Z*-1**, ***Z*-2** and ***Z*-3** to adopt several conformations with distinct orientation of dihydroxycarboxylic and heterocyclic moieties. The use of the modified Karplus equation proposed by Garbisch[23] allowed an assessment of the orientation of H5 with respect to H7. The $^4J_{H5-H7}$ allylic coupling constants of ca. 1 and 0 Hz are in agreement with torsion angles [H5–C5–C6–H6] of 0°±30° and 180°±30°, respectively. In addition, the same torsion angle can be estimated from the analysis of $^3J_{H5-H6}$ coupling constants—their values above 9 Hz suggest[24] two possible orientations along C5–C6 bond with torsion angles of approximately 0°±30° and 180°±30°. Consequently, the observation of $^4J_{H5-H7}$ long-range coupling constants in ***Z*-1**, ***Z*-2** and ***Z*-3** suggested *anti* orientation of H5 and H6 along C5–C6 bond in the major rotamers and *syn* orientation in the minor rotamers with W-geometry along the H5–C5–C6=C7–H7 bonds in the latter. Interestingly, only one set of signals was observed for each of ***E*-1**, ***E*-2** and ***E*-3**. The observed multiplicity pattern of *E*-isomers is in accordance with a W-geometry arrangement between H5 and H7 protons, where H5 and H6 protons have an *anti* orientation across the C5–C6 bond.

The observed differences in the $^4J_{H5-H7}$ allylic coupling constants and distinct cross-peak intensities in the NOESY spectra of the major and minor rotamers along the C5–C6 bond were used for their identification. The key differences in the volumes of NOESY cross-peaks were observed between H5 and H7 protons with respect to the protons of fluorophenyl and isopropyl groups of ***Z*-1**, ***Z*-2** and ***Z*-3**. In the case of ***Z*-1**, the major rotamer showed a very strong NOESY cross-peak between H7 and the *o*-fluorophenyl protons, whereas a weak cross-peak was observed between H5 and the *o*-fluorophenyl protons (Fig. 4a). In full support, a strong NOESY interaction was noted between H7 and the tertiary proton of the isopropyl group, which exhibits NOESY cross-peak of moderate intensity with H5 as well. In addition, the orientation of H5 is defined by its NOESY signal with the methyl protons of the isopropyl group. The above spatial proximities are consistent with an *anti* orientation of H5–C5 and H7–C7 bonds observed in the lowest energy structure of ***Z*-1** as calculated by DFT calculations (Fig. 4a).

In contrast, no NOESY cross-peaks were observed between H5 and the isopropyl protons for the minor rotamer of ***Z*-1**. This observation is in agreement with the DFT optimized structure of ***Z*-1** presented in Fig. 4b. The orientation of H5 away from the isopropyl group attached to C6′ is supported by moderate NOESY cross-peaks between H5 and *o*-fluorophenyl protons as well as between H7 and fluorophenyl, and strong NOESY interaction between H7 and isopropyl protons. The conformational features of minor rotamer of ***Z*-1** are in agreement with the *syn* orientation of H5 and H6 along the C5–C6 bond (Fig. 4b).

Higher rotational flexibility and consequently lower mole fractions of minor conformers of ***Z*-2** and ***Z*-3** prevented detailed conformational analysis based on NOESY experiments. Nevertheless, the proposed *anti* orientation of H5 and H6 along the C5–C6 bond in the major rotamer and *syn* orientation in the minor rotamer is in good agreement with the energetic preferences across C5–C6 bond of *Z*-rosuvastatin derivatives (vide infra).

The dynamic equilibrium between the two conformers, M⇄m, was evaluated on the basis of their mole fractions, which were estimated by the integral values of well-resolved H7 proton signals at five different temperatures in the range from 223 to 263 K (Fig. 3). As the temperature increased, the population of conformer m increased with respect to conformer M (Table 2). Thermodynamic parameters for ***Z*-1**, ***Z*-2** and ***Z*-3** were obtained from van't Hoff plots (Fig. 5). The slope of the lines in van't Hoff plots suggested the predominance of enthalpy contributions in controlling the dynamic equilibria M⇄m for each of ***Z*-1**, ***Z*-2** and ***Z*-3** (Table 2).

The experimental observations on the conformational equilibria between rotamers M and m were augmented by quantum mechanical calculations at B3LYP/6-311+G(d,p) level of theory using Gaussian 09 program.[25] Torsion angle θ [H5–C5–C6–H6] was defined to follow energetic variations induced by reorientation around the C5–C6 bond in ***Z*-1**, ***Z*-2** and ***Z*-3**. The relative energy profile along torsion angle θ with 30° resolution shows that the rotamer with the lowest energy adopts an *anti* orientation of H5 and H6 across the C5–C6 bond (Fig. 6a). Energy minimization of *anti* and *syn* rotamers of ***Z*-1** in the local energy minima established by energy profile calculations were performed without any constraints; *anti* rotamer of ***Z*-1** exhibited the lowest energy, while the *syn* rotamer showed 1.7 kcal mol^{-1} higher energy. The torsion angles θ of freely optimized *anti* and *syn* rotamers of ***Z*-1** were 179.4°

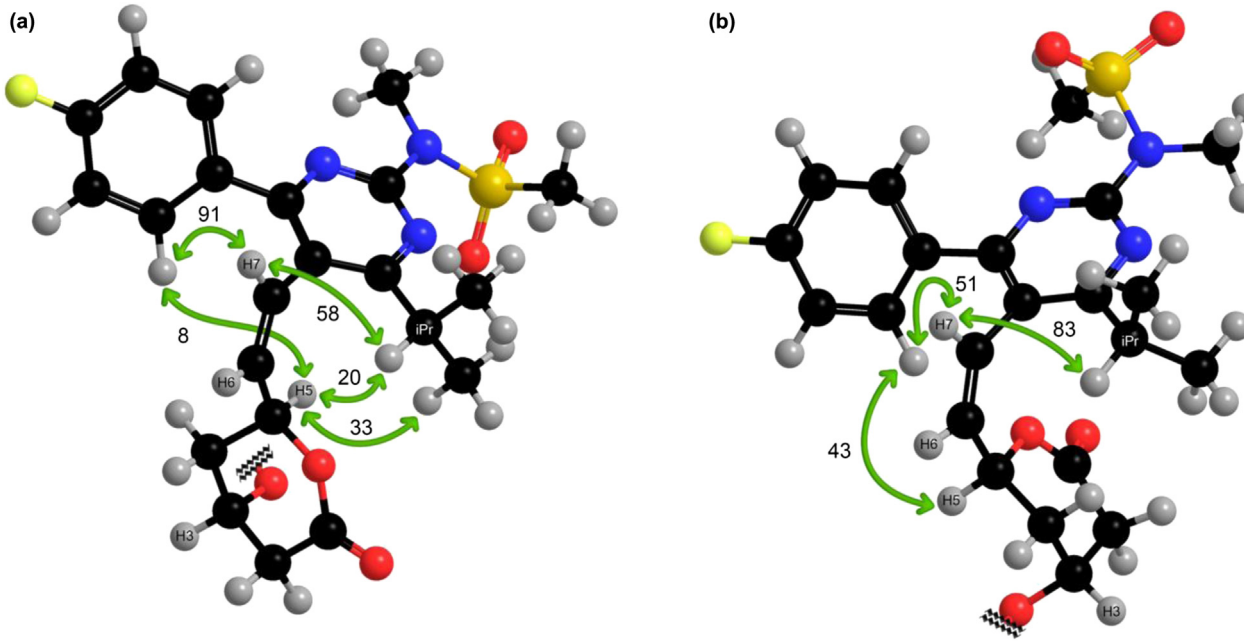

Fig. 4. Freely optimized structures of ***Z*-1** at B3LYP/6-311+G(d,p) level of theory with *anti* (a) and *syn* (b) orientations of H5 and H6 protons along the C5–C6 bond. The key NOESY signals from a NOESY spectrum (mixing time 200 ms, 253 K) are marked with green arrows. Numbers correspond to relative integral volumes with respect to H6–H7 cross-peak, which is arbitrarily set to 100 units. For clarity *tert*-butyldimethylsilyl group attached to C3 is not shown.

Table 2
Temperature variation of conformer population and thermodynamic parameters for dynamic equilibria of ***Z*-1**, ***Z*-2** and ***Z*-3**

Compound	Mole fractions of minor conformers					Thermodynamic parameters[a]		
	223 K	233 K	243 K	253 K	263 K	ΔH°	$-T\Delta S^\circ$	ΔG°
***Z*-1**[b]	0.246	0.266	0.278	0.299	0.307	0.90	−0.55	0.35
***Z*-2**[b]	0.123	0.143	0.175	0.201	0.227	2.20	−1.77	0.43
***Z*-3**[c]	0.154	0.163	0.176	0.209	0.231	1.50	−0.97	0.53

[a] Reported in kcal mol^{-1}.
[b] Compound dissolved in acetone-d_6.
[c] Compound dissolved in methanol-d_4.

and 48.6°, respectively. The respective rotational energy barrier of 5.2 kcal mol^{-1} along the torsion angle θ was found at θ=330°. Noteworthy, conformational features of energetically optimized rotamers are in good agreement with NOESY intensities and $^4J_{H5-H7}$ allylic coupling constants, where rotamer M exhibits *anti* orientation and rotamer m corresponds to a *syn* orientation of H5 and H6 along the C5–C6 bond.

Two minima were found for an *anti* orientation of H5 and H6 along the C5–C6 bond in ***Z*-2** with low rotational energy barrier of 2.1 kcal mol^{-1} (Fig. 6a). The *syn* rotamer of ***Z*-2** exhibited significantly higher energy with respect to the global minimum (5.3 kcal mol^{-1}). Similarly, the two minima with the low rotational energy barrier were observed in *anti* region for ***Z*-3**. Rotamer of ***Z*-3** with *syn* orientation of H5 and H6 along the C5–C6 bond exhibited higher energy of 3.8 kcal mol^{-1}. ***Z*-1**, ***Z*-2** and ***Z*-3** showed rotational energy barriers of 4.9–6.4 kcal mol^{-1} between *syn* and *anti* rotamers along the C5–C6 bonds.

E-isomers exhibit the lowest energies in *syn* region of ***E*-1**, ***E*-2** and ***E*-3** (Fig. 6b). The low rotational energy barrier of ca. 2 kcal mol^{-1} is consistent with a single set of signals observed in ^{1}H NMR spectra.

The coalescence temperatures enabled estimation of exchange rates k_E and $\Delta G^\ddagger$ for rotational energy barriers using the Eyring equation (Table 3).

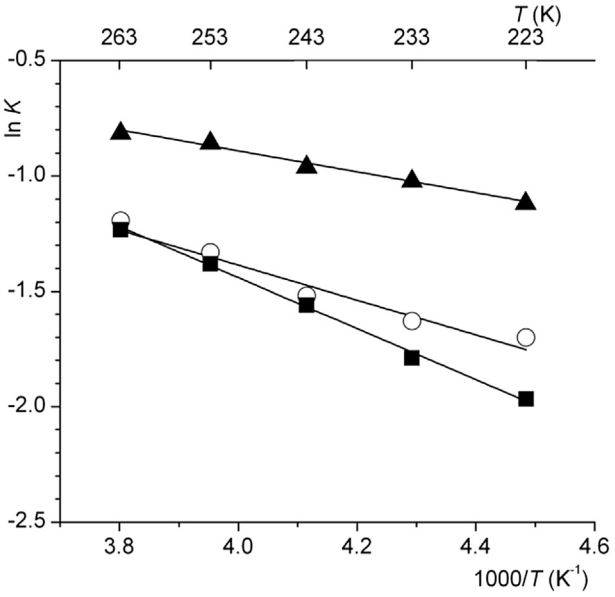

Fig. 5. Van't Hoff plots for equilibrium M⇄m of ***Z*-1** (▲), ***Z*-2** (■) and ***Z*-3** (○) in the temperature range from 223 to 263 K. The straight lines are the best fits to the experimental data using least-square method (Pearson correlation coefficient R^2 was 0.9879, 0.9968 and 0.9439 for ***Z*-1**, ***Z*-2** and ***Z*-3**, respectively). The mean-square deviations were below 0.003 with the largest individual deviation below 0.05.

The values of rotational energy barriers along the C5–C6 bonds in ***Z*-1**, ***Z*-2** and ***Z*-3** from ab initio calculations were between 4.9 and 6.4 kcal mol^{-1} (Fig. 6). In contrast, the experimentally determined rotational energy barriers were much larger—between 14.4 and 14.8 kcal mol^{-1} (Table 3). The above discrepancies implied that another conformationally flexible bond is important for observation of two rotamers at low temperatures. Since the C6=C7 double bond is tilted with respect to the aromatic plane and the two sides of aromatic ring are different, the rotation along the C5′–C7 bond would generate a pair of atropisomers. Further exploration focused

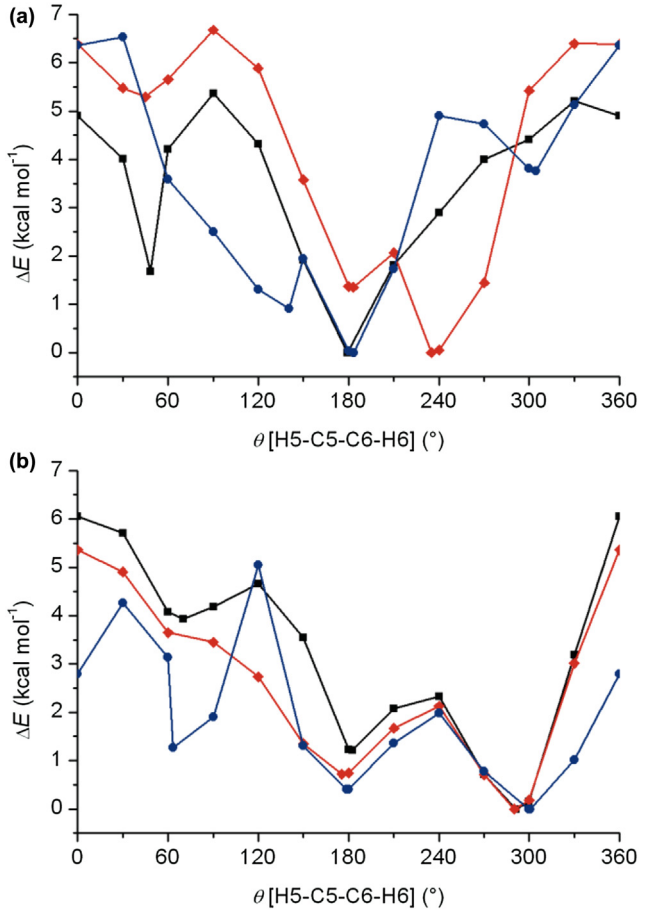

Fig. 6. Relative potential energy of ***Z*-1** (■), ***Z*-2** (◆) and ***Z*-3** (●) in (a) and of ***E*-1** (■), ***E*-2** (◆) and ***E*-3** (●) in (b) as a function of the [H5–C5–C6–H6] torsion angle at the B3LYP/6-311+G(d,p) level of theory.

Table 3
Exchange rates k_E and $\Delta G^{\ddagger}$ for rotational energy barriers of ***Z*-1**, ***Z*-2** and ***Z*-3**[a]

Compound	$\Delta\nu$ (Hz)	k_E (s^{-1})	$\Delta G^{\ddagger}$ (kcal mol^{-1})
***Z*-1**[b]	58.0	129	14.8
***Z*-2**[b]	127.5	283	14.4
***Z*-3**[c]	91.2	203	14.6

[a] The coalescence temperature for ***Z*-1**, ***Z*-2** and ***Z*-3** was estimated to be 303 K.
[b] Compound dissolved in acetone-d_6.
[c] Compound dissolved in methanol-d_4.

solely on ***Z*-1** because NOESY experiments prevented detailed conformational analysis of ***Z*-2** and ***Z*-3**. Four major energetically preferred conformations are expected for ***Z*-1** with respect to rotations along C5–C6 and C5′–C7 single bonds (Fig. 7).

Torsion angle ϕ [C6′–C5′–C7–H7] was defined and its potential energy profile was calculated for ***Z*-1** with 30° resolution at B3LYP/6-311+G(d,p) level of theory. During the energy profile calculations the torsion angle θ (rotation along C5–C6 bond) was set both to *anti* and *syn* orientations. It turned out that when the torsion angle θ was set in *syn* orientation, the rotation along the C5′–C7 bond exhibited very high energy barrier. Relative potential energy profile of ***Z*-1** as a function of the torsion angle ϕ, where torsion angle θ was in *anti* orientation, showed two minima at ϕ=60° and ϕ=240°, which suggests presence of atropisomers (Fig. 8). Rotational energy barrier along C5′–C7 bond is 12.7 kcal mol^{-1}, which is in good agreement with experimentally determined rotational energy barrier (Table 3). Two out of the four major possible conformers

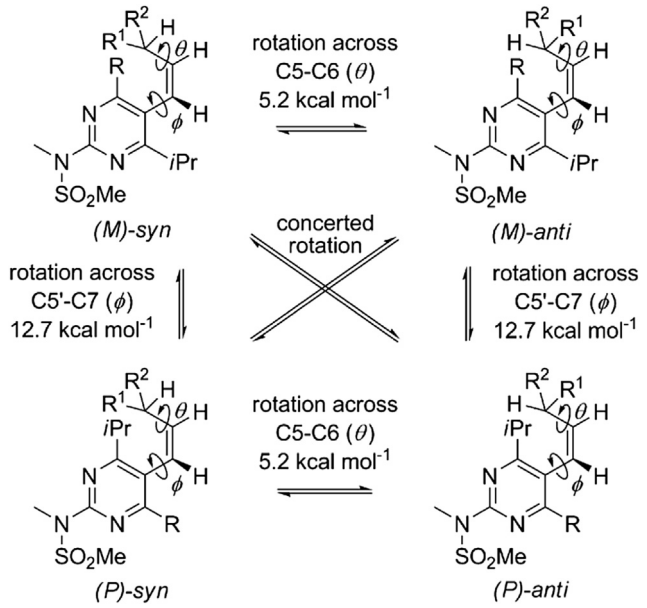

Fig. 7. Four major energetically favourable conformers of ***Z*-1** (R=*p*-F–C_6H_4, R^1 and R^2 represent the lactone moiety) with the corresponding rotational energy barriers across C5′–C7 and C5–C6 bonds.

that were observed in NMR spectra at lower temperatures most probably correspond to one of the diagonal pairs shown in Fig. 7 ((*M*)-*syn* and (*P*)-*anti* or (*M*)-*anti* and (*P*)-*syn*), with concerted rotation along two single bonds of ***Z*-1**. However, on the basis of *J* coupling constants and NOESY experiments it could not be determined, which diagonal pair presented in Fig. 7 is present in the solution.

Conformational analysis together with thermodynamic preferences of *Z*-isomeric rosuvastatin analogues provides insight into conformational variability that is important for studying potential interactions within the HMGR binding site. A recent study combining theoretical and experimental methods showed that an inhibitory peptide causes ordering of secondary structure of HMGR upon binding,[26], which implies that a wide variety of molecules could bind to the active site of HMGR and the newly synthesized *Z*-isomers of rosuvastatin are not excluded.

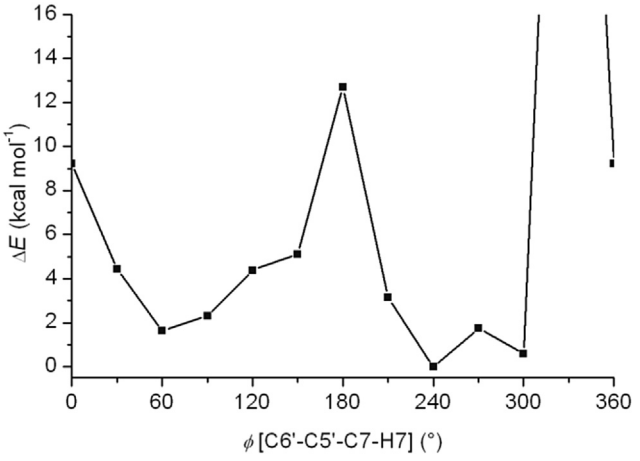

Fig. 8. Relative potential energy of ***Z*-1** as a function of the ϕ [C6′–C5′–C7–H7] torsion angle at the B3LYP/6-311+G(d,p) level of theory. The torsion angle θ [H5–C5–C6–H6] was set to *anti* orientation. Rotation between ϕ=300° and ϕ=360° led to very high energy.

3. Conclusion

Both *Z*- and *E*-isomers of rosuvastatin and its lactonized analogues were prepared and characterized by heteronuclear NMR spectroscopy. The NMR resonance line broadening in ^{1}H NMR spectra observed for *Z*-isomeric rosuvastatin analogues at room temperature originates from the dynamic exchange between the two conformers. In contrast, isomers ***E*-1**, ***E*-2** and ***E*-3** exhibit a single set of narrow NMR resonances. The two conformers of *Z*-isomers were distinguished at low temperature, where well-defined differences in $^4J_{H5-H7}$ allylic coupling constants between major and minor conformers suggested the presence of two rotamers of ***Z*-1** along the C5–C6 single bond. An *anti* orientation of H5 and H6 along the C5–C6 bond was assigned to the major rotamer, whereas the minor rotamer exhibited a *syn* orientation. Thermodynamic preferences between the two conformers were assessed with ^{1}H NMR experiments over a temperature range from 223 to 263 K. An increase in the sample temperature was followed by an increase in the population of the minor conformer. Additionally, two conformers observed in the NMR spectra at lowered temperature most likely correspond to a pair of atropisomers, where concerted rotation along both C5–C6 and C5′–C7 bonds is supported by experimentally determined as well as by calculated rotational energy barrier.

4. Experimental section

4.1. General

Reagents and solvents were acquired from commercial sources and used without further purification. Reactions were monitored by using analytical TLC plates (Merck; silica gel 60 F_{254}, 0.25 mm), and compounds were visualized with UV radiation. Silica gel grade 60 (70–230 mesh, Merck) was used for column chromatography. Melting points were determined with a Mettler Toledo DSC822^e apparatus (heating rate 10 °C/min) and are referred to as onset values and peak values. Optical rotations were measured on a Perkin Elmer 341-series polarimeter; only noteworthy absorptions are listed. High-resolution mass spectra were obtained with a VG-Analytical AutospecQ instrument and a Q-TOF Premier instrument.

4.2. NMR experiments

^{1}H and ^{13}C NMR spectra were acquired on Agilent Technologies (Varian) VNMRS 600 MHz, Unity Inova 300 MHz and DD2 300 MHz NMR spectrometers. Sample concentrations used in NMR studies were ca. 20 mM dissolved in acetone-d_6 or methanol-d_4. Two-dimensional homonuclear (COSY, NOESY) and heteronuclear (HSQC, HMBC) NMR experiments with gradients were used to structurally elucidate rosuvastatin analogues. 2D NOESY experiments were performed using a mixing time of 200 ms, which ensures the operation in the initial linear part of the NOESY buildup curve.

4.3. Ab initio calculations

Initial structures were generated by Chem3D Pro 10.0 software and energy minimization at B3LYP/6-311+G(d,p) level was performed without any constraints for *anti* orientation along the C5–C6 bond using Gaussian 09.[25] Torsion angles θ [H5–C5–C6–H6] and ϕ [C6′–C5′–C7–H7] were defined to follow energetic changes induced by reorientation. The relative energy profile of the torsion angles θ and ϕ were calculated with 30° resolution, where orientations were restrained along [H5–C5–C6–H6] and [C6′–C5′–C7–H7] torsion angles, respectively, while other degrees of freedom were freely optimized. Frequency calculations verified that the optimized geometries at (local) minima were stable points on the potential energy surface. Note that structure calculations for ***Z*-3** and ***E*-3** were performed on their acidic forms with COOH groups.

4.4. Synthetic procedures

*4.4.1. Synthesis of N-(4-(4-fluorophenyl)-5-((Z)-2-((2S,4R)-4-hydroxy-6-oxotetrahydro-2H-pyran-2-yl)vinyl)-6-isopropylpyrimidin-2-yl)-N-methylmethanesulfonamide (**Z-2**).* A solution of tetrabutylammonium fluoride trihydrate (191 mg, 0.61 mmol; 1.75 equiv) and AcOH (95 μL, 1.66 mmol; 4.8 equiv) in THF (2 mL) was cooled in an ice bath. Then a solution of ***Z*-1**[21] (200 mg, 0.35 mmol) in THF (2 mL) was added. The solution was left to stir for 22 h at room temperature. The solvent was evaporated under reduced pressure and the residue was dissolved in EtOAc (5 mL). The organic layer was washed with water (5 mL), saturated solution of $NaHCO_3$ (5 mL), brine (5 mL) and water (5 mL), respectively. Combined organic layers were dried over Na_2SO_4 and evaporated under reduced pressure. The residue was purified by column chromatography (silica gel, EtOAc–Hex, 1:1) to give 89 mg (55% yield) of pure ***Z*-2**; mp 188.6 °C (onset), 198.0 °C (peak); $[\alpha]_D^{25}$ +126 (*c* 0.25, MeOH); ν_{max} (KBr) 3444, 2969, 2932, 1735, 1606, 1548, 1511, 1371, 1230, 1155, 962, 769, 567, 521 cm^{-1}; δ_H (600 MHz, acetone-d_6) 7.82 (2H, b, 4-F–C_6H_4), 7.22 (2H, b, 4-F–C_6H_4), 6.89 (1H, b, H-7), 5.79 (1H, b, H-6), 4.82 (1H, b, H-5), 4.23 (1H, b, OH), 4.12 (1H, b, H-3), 3.54 (6H, s, N–CH_3 and SO_2–CH_3), 3.36 (1H, b, C*H*$(CH_3)_2$), 2.55 (1H, dd, *J* 17.6, 4.1 Hz, H-2a), 2.38–2.32 (1H, m, H-2b), 1.56–1.42 (1H, m, H-4a), 1.30 (3H, d, *J* 6.5 Hz, CH(C*H*$_3)_2$), 1.26 (3H, d, *J* 6.5 Hz, CH(C*H*$_3)_2$), 0.82 (1H, b, H-4b); δ_C (75 MHz, acetone-d_6) 175.9 (C-6′), 169.4 (C-1), 164.6 (C-4′), 164.4 (d, J_{CF} 248.0 Hz, 4-F–C_6H_4), 159.3 (C-2′), 135.5 (d, J_{CF} 3.3 Hz, 4-F–C_6H_4), 133.7 (C-6), 133.2 (d, J_{CF} 8.7 Hz, 4-F–C_6H_4), 127.9 (C-7), 120.2 (C-5′), 115.9 (d, J_{CF} 21.7 Hz, 4-F–C_6H_4), 72.9 (C-5), 62.8 (C-3), 42.4 (SO_2–CH_3), 39.3 (C-2), 34.8 (C-4), 33.7 (N–CH_3), 33.5 (*C*H$(CH_3)_2$), 22.0 (CH(*C*H$_3)_2$), 21.4 (CH(*C*H$_3)_2$); HRMS (ESI): MH^+, found: 464.1647. $C_{22}H_{27}FN_3O_5S$ requires 464.1650.

*4.4.2. Synthesis of (3R,5S,Z)-7-(4-(4-fluorophenyl)-6-isopropyl-2-(N-methylmethylsulfonamido)pyrimidin-5-yl)-3,5-dihydroxyhept-6-enoate calcium (**Z-3**).* To a solution of ***Z*-2** (139 mg, 0.30 mmol) in THF–water, 4:1 (5 mL) at 30 °C was added 2 M aqueous NaOH (161 μL, 0.32 mmol, 1.075 equiv). After 2 h the reaction was finished and THF was evaporated under reduced pressure. To a 2 mL of an aqueous solution of the sodium salt of *Z*-isomeric rosuvastatin was added a solution of $CaCl_2$ (70 mg, 0.60 mmol; 2 equiv) in water (2 mL). The resulting white precipitation was left to stir at rt for 18 h. Then it was filtered off, washed with water (3×5 mL) and dried at 60 °C under vacuum to give 48 mg (64% yield) of pure ***Z*-3**; $[\alpha]_D^{25}$ +30.8 [*c* 0.25, MeOH]; ν_{max} (KBr) 3426, 2969, 2932, 1605, 1549, 1511, 1439, 1394, 1370, 1336, 1228, 1155, 963, 771, 575, 521, 508 cm^{-1}; δ_H (600 MHz, methanol-d_4) 7.79 (2H, b, 4-F–C_6H_4), 7.17 (2H, b, 4-F–C_6H_4), 6.64 (1H, b, H-7), 5.62 (1H, b, H-6), 4.53 (2H, b, OH ×2), 3.84 (1H, b, H-5), 3.79 (1H, b, H-3), 3.55 (3H, s, N–CH_3), 3.52 (3H, s, SO_2–CH_3), 3.38 (1H, b, C*H*$(CH_3)_2$), 2.01 (1H, b, H-2a), 1.96 (1H, b, H-2b), 1.30 (3H, b, CH(C*H*$_3)_2$), 1.28 (3H, b, CH(C*H*$_3)_2$), 1.27 (1H, b, H-4a), 0.25 ppm (1H, b, H-4b); δ_C (75 MHz, methanol-d_4) 181.6 (C-1), 176.8 (C-6′), 164.9 (C-4′), 164.9 (d, J_{CF} 249.2 Hz, 4-F–C_6H_4), 159.4 (C-2′), 137.5 (C-6), 135.9 (d, J_{CF} 3.4 Hz, 4-F–C_6H_4), 133.4 (d, J_{CF} 8.4 Hz, 4-F–C_6H_4), 124.8 (C-7), 121.2 (C-5′), 116.1 (d, J_{CF} 21.8 Hz, 4-F–C_6H_4), 69.4 (C-3), 68.4 (C-5), 44.8 (C-2), 42.4 (C-4), 42.3 (SO_2–CH_3), 33.8 (N–CH_3 and *C*H$(CH_3)_2$), 22.7 (CH(*C*H$_3)_2$), 22.0 ppm (CH(*C*H$_3)_2$); HRMS (ESI): MH^+, found: 482.1750. $C_{22}H_{29}FN_3O_6S$ requires 482.1756.

Acknowledgements

This work was supported by the Slovenian Research Agency (ARRS, Grant Nos. P1-0242 and J1-4020), EU FP7 projects with

acronyms EAST-NMR (Grant No. 228461) and Bio-NMR (Grant No. 261863). We gratefully acknowledge Dr. I. Gazić Smilović for valuable discussions; L. Kolenc, S. Borišek and M. Borišek for assistance in some analytical work; Dr. M. Črnugelj, A. Gaćeša and M. Friedrich for acquiring some NMR spectra; Dr. D. Urankar and Prof. J. Košmrlj for HRMS analysis. J. Fabris thanks Public Agency for Technology of the Republic of Slovenia (TIA) for young researcher fellowship (MR-10/75). Operation part financed by the European Union, European Social Fund.

Supplementary data

Supplementary data associated with this article can be found in the online version. It contains ^{1}H NMR spectrum of ***Z*-3** in methanol-d_4 at 328 K, freely optimized structure of ***Z*-2** at the B3LYP/6-311+G(d,p) level of theory with *anti* orientation along C5–C6 bond, ^{1}H and ^{13}C NMR spectra for ***Z*-2** and ***Z*-3**, Cartesian coordinates of energy optimized structures at B3LYP/6-311+G(d,p) level. Supplementary data related to this article can be found at http://dx.doi.org/10.1016/j.tet.2013.05.020.

References and notes

1. Desai, D. A.; Zakaria, S.; Ouyang, P. *Curr. Atheroscler. Rep.* **2012**, *14*, 17–25.
2. Zhang, K. Z.; Kaufman, R. J. *Nat. Cell Biol.* **2003**, *5*, 769–770.
3. Singh, N.; Tamariz, J.; Chamorro, G.; Medina-Franco, J. L. *Mini-Rev. Med. Chem.* **2009**, *9*, 1272–1283.
4. (a) Endo, A.; Kuroda, M.; Tsujita, Y. *J. Antibiot.* **1976**, *29*, 1346–1348; (b) Endo, A.; Tsujita, Y.; Kuroda, M.; Tanzawa, K. *Eur. J. Biochem.* **1977**, *77*, 31–36.
5. Alberts, A. W.; Chen, J.; Kuron, G.; Hunt, V.; Huff, J.; Hoffman, C.; Rothrock, J.; Lopez, M.; Joshua, H.; Harris, E.; Patchett, A.; Monaghan, R.; Currie, S.; Stapley, E.; Albers-Schonberg, G.; Hensens, O.; Hirschfield, J.; Hoogsteen, K.; Liesch, J.; Springer, J. *Proc. Natl. Acad. Sci. U.S.A.* **1980**, *77*, 3957–3961.
6. Tsujita, Y.; Kuroda, M.; Shimada, Y.; Tanzawa, K.; Arai, M.; Kaneko, I.; Tanaka, M.; Masuda, H.; Tarumi, C.; Watanabe, Y.; Fujii, S. *Biochem. Biophys. Acta* **1986**, *877*, 50–60.
7. Hoffman, W. F.; Alberts, A. W.; Anderson, P. S.; Chen, J. S.; Smith, R. L.; Willard, A. K. *J. Med. Chem.* **1986**, *29*, 849–852.
8. Tse, F. L. S.; Smith, H. T.; Ballard, F. H.; Nicoletti, J. *Biopharm. Drug Dispos.* **1990**, *11*, 519–531.
9. Ferguson, E.; McNally, W.; Bocan, T. M. A.; Uhlendorf, P. D.; Krause, B. R.; Sliskovic, D. R.; Obrien, P.; Roth, B. D.; Newton, R. S. *FASEB J.* **1991**, *5* A1253–A1253.
10. Quirk, J.; Thornton, M.; Kirkpatrick, P. *Nat. Rev. Drug Discovery* **2003**, *2*, 769–770.
11. Kajinami, K.; Mabuchi, H.; Saito, Y. *Expert Opin. Invest. Drugs* **2000**, *9*, 2653–2661.
12. Časar, Z. *Curr. Org. Chem.* **2010**, *14*, 816–845.
13. Kant, J. *J. Org. Chem.* **1993**, *58*, 2296–2301.
14. Onodera, S.; Nishida, K.; Takeuchi, K. *Drug Des. Rev.* **2004**, *1*, 133–144.
15. (a) Cirla, A.; Mann, J. *Nat. Prod. Rep.* **2003**, *20*, 558–564; (b) Shirai, R.; Okabe, T.; Iwasaki, S. *Heterocycles* **1997**, *46*, 145–148.
16. Simmons, D. L.; Botting, R. M.; Hla, T. *Pharmacol. Rev.* **2004**, *56*, 387–437.
17. Stokker, G. E.; Hoffman, W. F.; Alberts, A. W.; Cragoe, E. J.; Deana, A. A.; Gilfillan, J. L.; Huff, J. W.; Novello, F. C.; Prugh, J. D.; Smith, R. L.; Willard, A. K. *J. Med. Chem.* **1985**, *28*, 347–358.
18. Beck, G.; Kesseler, K.; Baader, E.; Bartmann, W.; Bergmann, A.; Granzer, E.; Jendralla, H.; Vonkerekjarto, B.; Krause, R.; Paulus, E.; Schubert, W.; Wess, G. *J. Med. Chem.* **1990**, *33*, 52–60.
19. Istvan, E. S.; Deisenhofer, J. *Science* **2001**, *292*, 1160–1164.
20. (a) Holdgate, G. A.; Ward, W. H. J.; McTaggart, F. *Biochem. Soc. Trans.* **2003**, *31*, 528–531; (b) da Costa, R. F.; Freire, V. N.; Bezerra, E. M.; Cavada, B. S.; Caetano, E. W. S.; de Lima Filho, J. L.; Albuquerque, E. L. *Phys. Chem. Chem. Phys.* **2012**, *14*, 1389–1398.
21. Časar, Z.; Steinbücher, M.; Košmrlj, J. *J. Org. Chem.* **2010**, *75*, 6681–6684.
22. (a) Časar, Z. *Synlett* **2008**, 2036–2040; (b) Časar, Z.; Košmrlj, J. *Synlett* **2009**, 1144–1148; (c) Cluzeau, J.; Časar, Z.; Mrak, P.; Ošlaj, M.; Kopitar, G. WO 2009092702, *Chem. Abstr.* **2009**, *151*, 218948; (d) Časar, Z.; Tramšek, M.; Goršek, A. *Acta Chim. Slov.* **2010**, *57*, 66–76; (e) Troiani, V.; Cluzeau, J.; Časar, Z. *Org. Process Res. Dev.* **2011**, *15*, 622–630.
23. Garbisch, E. W. *J. Am. Chem. Soc.* **1964**, *86*, 5561–5564.
24. Haasnoot, C. A. G.; de Leeuw, F. A. A. M.; Altona, C. *Tetrahedron* **1980**, *36*, 2783–2792.
25. Frisch, M. J.; Trucks, G. W.; Schlegel, H. B.; Scuseria, G. E.; Robb, M. A.; Cheeseman, J. R.; Scalmani, G.; Barone, V.; Mennucci, B.; Petersson, G. A.; Nakatsuji, H.; Caricato, M.; Li, X.; Hratchian, H. P.; Izmaylov, A. F.; Bloino, J.; Zheng, G.; Sonnenberg, J. L.; Hada, M.; Ehara, M.; Toyota, K.; Fukuda, R.; Hasegawa, J.; Ishida, M.; Nakajima, T.; Honda, Y.; Kitao, O.; Nakai, H.; Vreven, T.; Montgomery, J. A.; Peralta, J. E.; Ogliaro, F.; Bearpark, M.; Heyd, J. J.; Brothers, E.; Kudin, K. N.; Staroverov, V. N.; Kobayashi, R.; Normand, J.; Raghavachari, K.; Rendell, A.; Burant, J. C.; Iyengar, S. S.; Tomasi, J.; Cossi, M.; Rega, N.; Millam, J. M.; Klene, M.; Knox, J. E.; Cross, J. B.; Bakken, V.; Adamo, C.; Jaramillo, J.; Gomperts, R.; Stratmann, R. E.; Yazyev, O.; Austin, A. J.; Cammi, R.; Pomelli, C.; Ochterski, J. W.; Martin, R. L.; Morokuma, K.; Zakrzewski, V. G.; Voth, G. A.; Salvador, P.; Dannenberg, J. J.; Dapprich, S.; Daniels, A. D.; Farkas, Ö.; Foresman, J. B.; Ortiz, J. V.; Cioslowski, J.; Fox, D. J. Wallingford CT, 2009.
26. Pak, V. V.; Koo, M.; Kim, M. J.; Yun, L.; Kwon, D. Y. *Bioorg. Med. Chem.* **2008**, *16*, 1309–1318.